**Advances in
Geosciences**

Exploitation of cloud top characterization from three-channel IR measurements in a physical PMW rain retrieval algorithm

F. Torricella, E. Cattani, and V. Levizzani

National Research Council, Institute of Atmospheric Sciences and Climate, Bologna, 40129, Italy

Abstract. Rainfall intensity estimates by passive microwave (PMW) measurements from space perform generally better over the sea surface with respect to land, due to the problems in separating true rain signatures from those produced by surfaces having similar spectral behaviour (e.g. snow, ice, desert and semiarid grounds). The screening procedure aimed at recognizing the various surface types and delimit precipitation is based on tests that rely on PMW measurements only and global thresholds. The shortcoming is that the approach tries to discard spurious precipitating features (often detected over the land-sea border) thus leading to *no-rain* conservative tests and thresholds. The TRMM mission, with its long record of simultaneous data from the Visible and Infrared Radiometer System (VIRS), the TRMM Microwave Imager (TMI) and rain profiles from the Precipitation Radar (PR) allows for unambiguous testing of the usefulness of cloud top characterization in rain detection.

An intense precipitation event over the North Africa is analysed exploiting a night microphysical RGB scheme applied to VIRS measurements to classify and characterize the components of the observed scenario and to discriminate the various types of clouds. This classification is compared to the rain intensity maps derived from TMI by means of the Goddard profiling algorithm and to the near-surface rain intensities derived from PR. The comparison allows to quantify the difference between the two rain retrievals and to assess the usefulness of RGB analysis in identifying areas of precipitation.

1 Introduction

Rainfall intensity estimates by passive microwave (PMW) measurements from space perform generally better over the sea surface with respect to land, due to the problems in separating true rain signatures from those produced by surfaces

Correspondence to: F. Torricella
(f.torricella@isac.cnr.it)

having similar spectral behavior (e.g., snow, ice, desert and semiarid grounds).

The initial screening procedure of a typical rain retrieval algorithm aimed at recognizing the various surface types and delimiting precipitation is based on tests that rely on PMW measurements only and on global derived thresholds. The shortcoming of this approach is well known: trying to discard spurious precipitating features leads to no-rain conservative tests and thresholds.

The use of other spectral regions to detect and characterize cloudy (and potentially precipitating) pixel areas can only be discouraged by the unavailability of time-space coincident multi-spectral measurements. The characterization of the cloud field by using time coincident – colocated visible (VIS) and infrared (IR) measurements prior to the application of the rain intensity retrieval algorithm can improve the selection of probably precipitating pixels.

The Tropical Rainfall Measurement Mission (TRMM) with its long record of coincident VIS, near infrared (NIR) and IR measurements taken by the Visible and Infrared Radiometer System (VIRS) and MW observations (from the TRMM Microwave Imager – TMI) complemented by the availability of validation rain data of the precipitation radar (PR) for a subset of observations, optimally allows for testing the usefulness of cloud top characterization in rain detection.

2 The study period

Summer 2002 was characterized by several extreme meteorological events in Europe and the Mediterranean area. Let us mention only the well known severe weather event that led to flooding in central Europe, most notably Germany, the Czech Republic and Austria, during the first half of August 2002. The event analyzed in this work took place several days after the central European disaster, on 22 to 29 August, pouring heavy rain in Italy, and causing local floods in Mallorca and important floods in Algeria, with tens of casualties, hundreds of homeless families, and severe social and
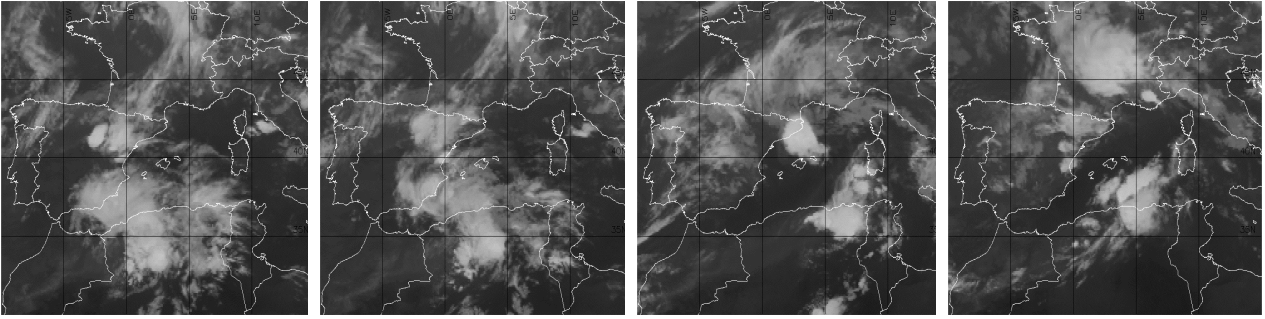
Fig. 1. METEOSAT-7 IR pictures for the study area. The selected slots are the nearest to the TRMM overpasses shown in Fig. 2, namely, from left to right, 23 August 22:00 UTC; 24 August 00:00 UTC; 24 August 23:00 UTC; 25 August 22:00 UTC.

economical damages. Torrential rains provoked heavy flooding in eastern Algeria, killing at least 10 people. Numerous buildings in the area were partially submerged.

Despite the significant duration of the event, characterized by several peaks of precipitation in different regions of Algeria, its sampling by TRMM instruments does not allow to properly follow the time evolution of the cloud systems. Moreover, due to the characteristics of the TRMM orbit, the whole western Mediterranean area was imaged only at nighttime, preventing a full exploitation of multispectral VIRS measurements.

The analysis of METEOSAT-7 IR images (Fig. 1) helps following the time evolution of the cloud field during one of the rain peaks, on 23, 24 and 25 August, characterized by the presence of strong convective cells over northeastern Spain, notably over Catalonia, Sardinia, central Italy, Balearic Islands and the north African coast. The movement during the three days span from northern Morocco to Tunisia with the development of very cold and active convective cells during both day- and nighttime.

3 Rain analysis from TMI and PR

The rain maps for the TRMM overpasses over the area for 23, 24 and 25 August are shown in Fig. 2. They are selected to be centered over Algeria and be characterized by heavy precipitation. All the TRMM passes over the area occurred at nighttime (from 22:30 to 00:30 UTC, local time being ~30′ later) during the three days. The rain intensity is retrieved from TMI measurements by means of the Goddard Profiling Algorithm version 6 (GPROF, Kummerow et al., 2001; McCollum and Ferraro 2003). All the TRMM data and products are obtained from the Distributed Active Archive Center of the Goddard Earth Sciences Data and Information Services Center of National Aeronautics and Space Administration. They are the version 6 reprocessed products 2A25 (precipitation radar rainfall rate and profile), 2A12 (hydrometeor profile), and 1B01 (calibrated radiance).

The GPROF algorithm calculates instantaneous rainfall rate estimates from the weighted average of rainfall rates from different vertical hydrometeor profiles created from numerical cloud models, primarily the Goddard Cumulus Ensemble model. Radiative transfer calculations for the frequencies and resolutions of a particular sensor are done to produce a library of vertical profiles with the associated brightness temperatures. The profiles used for estimation are chosen and given weights based on the proximity of the observed microwave radiances to those of the library of profiles. Then, in addition to a surface rainfall estimate, the estimated profiles can be used to estimate latent heating profiles for model assimilation. The physical concept of the GPROF algorithm is most effective over oceans, where the low and predictable oceanic emissivity results in information about ice and liquid hydrometeors over the range of microwave frequencies. On the other hand, the high and variable land surface emissivity makes the information from the low frequency channels ambiguous, so that the ice scattering at higher freqencies is currently the most useful way to estimate rainfall over land.

We considered the geographical area 25–40 N and 5 W–20 E and rain data were re-projected over a 0.1°×0.1° regular lat-lon grid. For each grid point the average rain rate from TMI and PR data were computed. At each grid point, 4 to 5 PR pixels and about 2 TMI pixels contributed to the average rain intensity value. Overall, PR detected 10 878 rainy pixels in the selected geographical area (out of which 1154 classified as convective) and TMI detected 5496 rainy pixels.

The scatter-plot in Fig. 3 reports the gridded rain intensity data of the whole event (38 orbits) derived from PR (x-axis) and TMI (y-axis). Depicted in blue are the values for all the rainy grid points (defined as grid mesh where PR detected at least one rainy pixel), and in red the subset of grid points classified by PR as convective (i.e. grid points where more than half PR pixels were classified as convective). The observation of rain maps and the scatter plot leads to the following remarks:

– in the common area of the swaths of the two instruments (widths: 878 km TMI, 247 km PR) TMI detected smaller rain areas than PR;
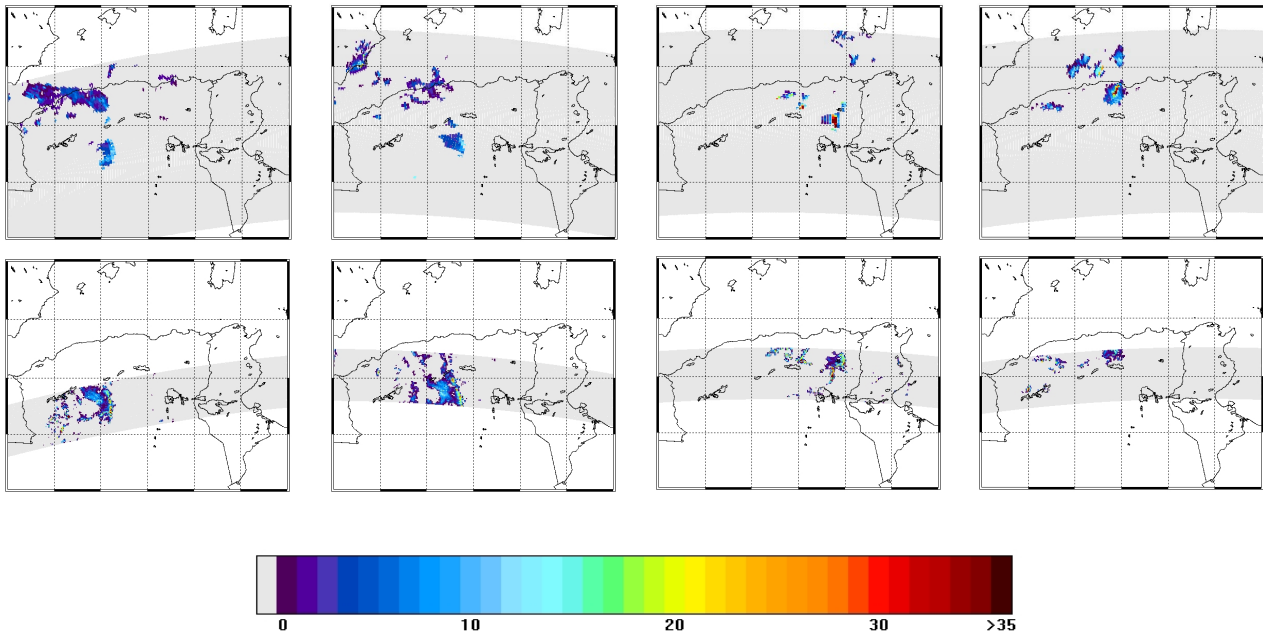
Fig. 2. Rain intensity maps (surface rain in mm h^{-1}) retrieved from TMI measurements (top) and from PR (bottom). Left to right: 23 August 22:50 LT; 24 August 00:27 LT; 24 August 23:40 LT; 25 August 22:50 LT.

– TMI overestimated light to medium rain intensities (*beamfilling* effect) and missed many rainy pixels;

– high rain intensities are in general underestimated by TMI;

– the majority of undetected rain areas (i.e. cases in which PR detect rain and the TMI algorithm revealed no precipitation) are classified by PR as convective;

– there are undetected rainy areas all over the rain intensity range, from 0 up to 25 mm h^{-1}.

4 Microphysical characterization of the cloud field

The RGB technique is a widely used method (Rosenfeld and Lensky, 1998; Kerkmann et al., 2004) that provides a relatively simple rendering of multispectral satellite information for the meteorological scenario interpretation.

The optimum coloring of the RGB image composites rely on the proper selection of the satellite sensor channels and the enhancement of the individual colors. The channel selection must be driven by the particular phenomenon (low or high clouds, dust, smoke etc.) to be emphasized in the satellite image. At the same time, the proper color enhancement requires the conversion from radiances to brightness temperatures (IR channels) or reflectances (VIS/NIR channels), selection of the display mode (inverted or not inverted), stretching of the dynamic range of the satellite data, and gamma correction.

The TRMM VIRS brightness temperatures at 3.75, 10.8 and 12 μm were used to product RGB images to describe
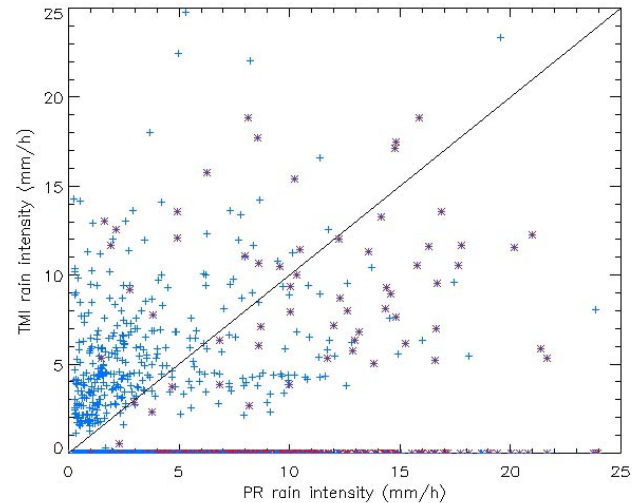
Fig. 3. Scatter plot of the gridded rain intensity as derived from PR (x-axis) and from TMI (y-axis). The surface rain intensities derived from the two instruments have been re-projected onto a regular lat-lon grid with resolution $0.1° \times 0.1°$. Blue symbols: all rainy pixels; red symbols: convective pixels.

the characteristics of the convective systems occurred during the study period. The adopted scheme, so-called *night microphysical*, was already applied to MSG SEVIRI images (Kerkmann et al., 2004), and is particularly recommended to emphasize the presence of high clouds during the night. According to this representation scheme the brightness temperature differences between 12 and 10.8 μm [BT(12)–BT(11)] are associated to the red beam with a recommended value

Table 1. Main features of the adopted night microphysical non inverted display.

Component	Channels	Range [K]
RED	BT(12)–BT(11)	[−4, 0]
GREEN	BT(11)–BT(3.7)	[−15, 6]
BLUE	BT(11)	[223, 293]

range from –4 to 0 K. They are sensitive to the cloud optical thickness and are characterized by small values for high cloud optical thickness. The brightness temperature differences between 10.8 and 3.75 μm [BT(11)–BT(3.7)] with its recommended range [−15, 6] K, depend on the cloud optical thickness, phase and particle size and are associated to the green beam in the RGB representation. Small or positive values are observed when an opaque scene (such as thick clouds or the surface) fills the field of view of the sensor. Positive differences occur over extended clouds due to the lower cloud emissivity at 3.75 μm (Ackerman et al., 1998). Finally, the brightness temperatures at 10.8 μm BT(11) in the recommended range from 223 to 293 K are a proxy for surface or cloud top temperatures and are represented by blue shades. For the VIRS RGB images the *non-inverted display mode* was selected, i.e. black corresponds to low signals and white to high signals. Table 1 reports the features of the adopted display scheme.

By using the described approach the maps shown in Fig. 4 have been produced for the four orbits of Fig. 2. Even if this kind of method requires an interpretation of the color shades, which is to some extent subjective and non-quantitative, it is apparent that in this case several categories of targets can be clearly detected in all the orbits, as follows:

- Desert soil in pink, characterized by small values of BT(12)–BT(11) and small values of BT(11)–BT(3.7), BT(11) ranging from 286 to 291 K.

- Sea surface in blue: BT(12)–BT(11) in the range [−2, −1] K, negative BT(11)–BT(3.7) in the range [−3,−1] K, BT(11)>293 K.

- Overshooting cloud tops in light green: small values of BT(12)–BT(11)> −1 K, high positive values of BT(11)–BT(3.7)≥6 K, BT(11)≤223 K.

- Cumulonimbus in orange: small BT(12)–BT(11)≥ −1 K, BT(11)–BT(3.7)< −10 K, BT(11)≤230 K.

- Dissipating cumulonimbus in dark red: BT(12)–BT(11) in the range [−3,−1] K, high negative values BT(11)–BT(3.7)≤ −15 K, BT(11) in the range [230, 245] K.

- Cirrus in dark blue: BT(12)–BT(11)≤ −2 K, high negative values of BT(11)–BT(3.7)≤ −15 K, BT(11) between 230 and 260 K.

In the RGB maps (Fig. 4) the white contour lines encompass areas where PR detected rain with intensity greater than 2 mm h^{-1}. Rainy areas are mainly correlated with light green shadows, or appear to be near the green spots. In some instances, isolated small precipitation areas appear also to be connected with the margins of the cloud field and to be characterized by not so bright green shadow.

5 Conclusion and outlook

Rain intensity maps were derived from TMI MW measurements by means of the physical GPROF version 6 algorithm. These rain data were compared to the near-surface rain intensity retrieved from PR measurements that was considered a reference data set. The swaths of the two instruments are quite different, so that direct comparison is restricted to the narrowest PR swath.

Visual inspection reveals that the main features of the precipitation field are well reproduced in the TMI data, but many small areas of precipitation go undetected, both isolated rainy pixels and areas connected with the border of the main precipitating area.

A systematic comparison conducted for all the 38 orbits during the study period helps in quantifying the differences between the two rain retrievals. Some of these differences can be due to the different resolution of the instruments (remember that the GPROF algorithm uses the low frequency channels, having ground spatial resolution as coarse as 30 km at 19 GHz, to be compared to the resolution of PR, 4.5 km). Moreover, the screening procedure that selects the possibly raining pixels is affected by well known shortcomings and limitations that often imply an underestimation of the rainy areas.

We analysed data of the co-located VIRS measurement to produce a classification of the components of the scenario and to discriminate the various types of clouds. This kind of analysis is useful for detecting cloudy areas probably associated with precipitation.

Due to the orbital characteristics of TRMM the whole severe event was imaged by the instruments only during the night, and this prevented the use of VIS and NIR channels, most useful for *quantitative* estimates of the cloud top characteristics (in terms of optical thickness and effective radius).

Nevertheless, the adopted *qualitative* RGB channel combination scheme allowed for some useful comments to be derived.

- Thick clouds are clearly delineated by the green-orange-red areas, while cold but non-precipitating thin clouds are characterized by blue tones.

- The precipitating areas detected by PR (encompassed by white contour lines in Fig. 4) are mainly connected with the light green color, characteristic of overshooting cloud tops, especially in the areas of maximum precipitation. Smaller precipitations areas on the downwind
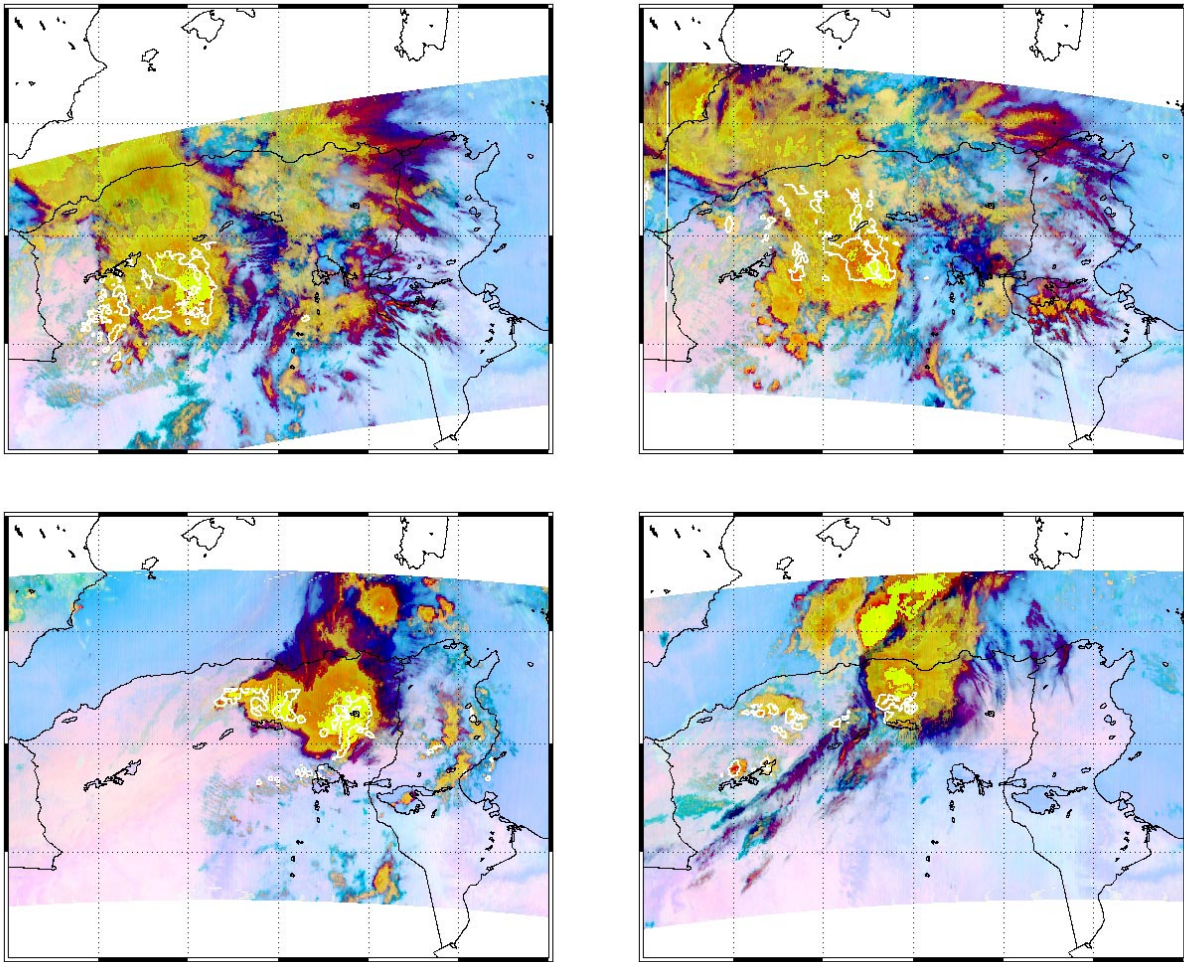
Fig. 4. RGB display scheme results for the orbits of Fig. 2. White contour lines encompass areas where PR detected a rain intensity greater than $2\,\mathrm{mm\,h^{-1}}$.

side of the cells do not strictly correlate with the green shade.

– The rainy areas outside the PR swath, detected by TMI also correlate with the green shade, but probably TMI does not properly detect rainy areas over the coast (see the area off the Algeria coast on orbit 22:50 on 25 August).

Edited by: V. Kotroni and K. Lagouvardos
Reviewed by: anonymous referee

References

Ackerman, S. A., Strabala, K. I., Menzel, W. P., Frey, R. A., Moeller, C. C., and Gumley, L. E.: Discriminating clear sky from clouds with MODIS, J. Geophys. Res., 103, 32 141–32 157, 1998.

Kerkmann, J., Lutz, H. J., König, M., Prieto, J., Pylkko, P., Roesli, H. P., Rosenfeld, D., Schmetz, J., and Zwatz-Meise, V.: MSG channels interpretation guide. Weather, surface conditions and atmospheric constituents, http://oiswww.eumetsat.org/WEBOPS/msg_interpretation/index.html, 2004.

Kummerow, C., Hong, Y., Olson, W. S., Yang, S., Adler, R. F., McCollum, J. R., Ferraro, R., Petty, G., and Wilheit, T. T.: The evolution of the Goddard Profiling Algorithm (GPROF) for rainfall estimation from passive microwave sensors, J. Appl. Meteor., 40, 1801–1820, 2001.

Mc Collum, J. R. and Ferraro, R.: Next generation of NOAA/NESDIS TMI, SSM/I, and AMSR-E microwave land rainfall algorithms, J. Geophys. Res., 108(D8), 8382, doi:10.1029/2001JD001512, 2003.

Rosenfeld, D. and Lensky, I. M.: Satellite-based insights into precipitation formation processes in continental and maritime convective clouds, Bull. Amer. Meteor. Soc., 79, 2457–2476, 1998.